J. Membrane Biol. 135, 83–92 (1993)

The Journal of
Membrane
Biology

Lateral Mobility of Lipid Analogues and GPI-Anchored Proteins in Supported Bilayers Determined by Fluorescent Bead Tracking

Martin Fein[1,2], Jay Unkeless[1], Frank Y.S. Chuang[1,3], Massimo Sassaroli[3], Rui da Costa[3], Heikki Väänänen[3], Josef Eisinger[3]

[1]Department of Biochemistry, Mount Sinai School of Medicine, New York, New York 10029
[2]Department of Biology, Bronx Community College-CUNY, New York, New York 10453
[3]Department of Physiology and Biophysics, Mount Sinai School of Medicine, New York 10029

Received: 15 December 1992/Revised: 22 February 1993

Abstract. Lipid analogues and glycosylphosphatidylinositol (GPI)-anchored proteins incorporated in glass-supported phospholipid bilayers (SBL) were coupled to small (30 nm diameter) fluorescent beads whose motion in the liquid phase was tracked by intensified fluorescence video microscopy. Streptavidin (St), covalently attached to the carboxyl modified surface of the polystyrene bead, bound either the biotinylated membrane component, or a biotinylated monoclonal antibody (mAb) directed against a specific membrane constituent. The positions of the beads tethered to randomly diffusing membrane molecules were recorded at 0.2 sec intervals for about 1 min. The mean square displacement (ρ) of the beads was found to be a linear function of diffusion time t, and the diffusion coefficient, D, was derived from the relation, $\rho(t) = 4Dt$. The values of D for biotinylated phosphatidylethanolamine (Bi-PE) dispersed in an egg lecithin : cholesterol (80 : 20%) bilayer obtained by this methodology range from 0.05 to 0.6 μm^2/sec with an average of $\langle D \rangle = 0.26$ μm^2/sec, similar to the value of $\langle D \rangle = 0.24$ μm^2/sec for fluorescein-conjugated phosphatidylethanolamine (Fl-PE) linked to St-coupled beads by the anti-fluorescein mAb 4-4-20 or its Fab fragment. These values of D are comparable to those reported for Fl-PE linked to 30 nm gold particles but are several times lower than that of Fl-PE in the same planar bilayer as measured by fluorescence photobleaching recovery, $D = 1.3$ μm^2/sec. The mobilities of two GPI-anchored proteins in similar SBL were also determined by use of the appropriate biotinylated mAb and were found to be $\langle D \rangle = 0.25$ and 0.56 μm^2/sec for the decay accelerating factor (DAF, CD55) and the human FcγRIIIB (CD16) receptors, respectively. The methodology described here is suitable for tracking any accessible membrane component.

Key words: Single particle tracking—Lateral diffusion—Fluorescent beads—Brownian motion—Fluorescence imaging—Membrane fluidity

Introduction

The dynamic properties of membranes have long been recognized as playing important roles in diverse membrane transport phenomena, including capping, receptor-mediated endocytosis and the aggregation of acetylcholine receptors during synapse formation (Taylor et al., 1971; Edwards & Frisch, 1976; Bretscher, 1984). These and similar phenomena suggest that the basic fluid mosaic model of the membrane (Singer & Nicholson, 1972) as a quasi-two-dimensional ideal solutions of lipids and proteins requires modification to allow for the existence of membrane domains and other heterogeneities that have the potential for guiding the diffusive motion of membrane components towards particular sites or in particular directions (Eisinger & Halperin, 1986; De Beus & Eisinger, 1992). Definitive experimental evidence for the existence of such membrane heterogeneities is still scant (Axelrod, 1983; Haverstick & Glaser, 1988; Rodgers & Glaser, 1991)

and single particle tracking (SPT)[1] methods such as the one described here may provide useful tools for investigating dynamic features of cell membranes and the motion and distribution of membrane constituents.

With SPT the lateral motion of a particle may be determined for a broad range of diffusion distances, whereas other experimental techniques yield values of D averaged over a characteristic distance: In fluorescence photobleaching recovery (FPR) (Axelrod et al., 1976), the diameter of the spot in which fluorescence bleaching and recovery are measured is usually of the order of a micrometer, and particles with shorter diffusion distances are lumped in the so-called "immobile fraction," since their exchange between the bleached and unbleached portions of the bilayer is largely unobserved. On the other hand, the excimer formation rate of pyrenyl probe molecules yields D for much shorter diffusion distances, of the order of a few nanometers (Eisinger, Flores & Petersen, 1986; Sassaroli et al., 1990). Indeed, while the diffusivities of lipid analogues measured by the two techniques differed little in *liquid-crystalline phase* bilayers, in *gel phase* bilayers the short range diffusivity of the pyrenyl probes was found to be two orders of magnitude greater than the FPR value (Fahey & Webb, 1978; Sassaroli et al., 1990). A diffusion distance dependence of D and of the mobile fraction of proteins in cell membranes has also been reported on the basis of an FPR study (Edidin & Stroynowski, 1991), again suggesting the existence of heterogeneities in membrane structure, dynamics and/or composition. The existence of persistent domains and corrals in membranes has also been suggested on the basis of other experiments (Yechiel & Edidin, 1987; Curtain, Gordon & Aloia, 1988; Edidin, Kuo & Sheetz, 1991; Rodgers & Glaser, 1991).

The most direct approach to investigating the mobility of a membrane molecule is by recording its trajectory with a suitable tracer. SPT was first introduced by Geerts *et al.* (1987) and has been implemented in various membrane systems by recording the motion of colloidal gold particles as tracers using contrast-enhanced bright field video microscopy (DeBrabander et al., 1991; Lee, Ishihara & Jacobson, 1991; Qian, Sheetz & Elson, 1991). It has also been used to track fluorescence-labeled LDL particles bound to LDL receptors and virus particles on the cell surface by means of fluorescence microscopy (Gross & Webb, 1988; Ghosh & Webb, 1990; Anderson et al., 1992). FPR methods generally provide the average diffusivity for an ensemble of molecules, while SPT is better suited to yield information about any heterogeneity of the diffusing species. SPT methods, moreover, appear to be superior to FPR for determining the range and directional preference of the diffusing particles.

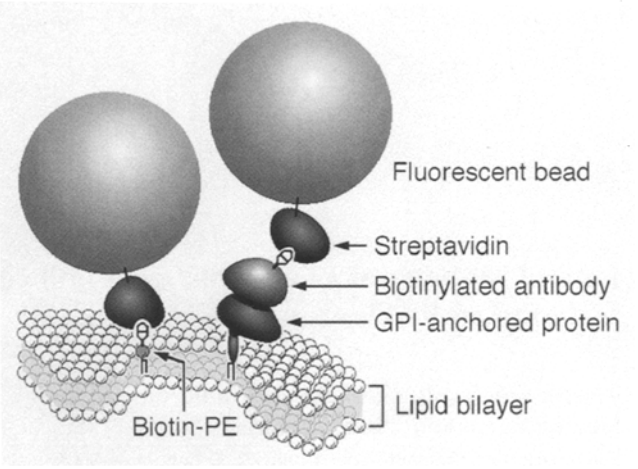

Fig. 1. Cartoon showing the linkage between Bi-PE (left), and a GPI-anchored protein (right) to streptavidin-conjugated microbeads. The molecular dimensions are approximately to scale. Note that the phosphoinositol moiety of GPI-anchored proteins is attached to the carboxy-terminal amino acid by a chain of five sugar moieties (Low, 1989).

In this paper, a general methodology is described for linking small fluorescent polystyrene beads to specific membrane components and for recording their motion by intensified fluorescence video microscopy. It is applied here to the investigation of the mobility of bead-tethered lipid analogues and glycosylphosphatidylinositol (GPI)-anchored proteins in glass-supported bilayers. The linkage between the tracer bead and the membrane molecule is provided by a streptavidin molecule covalently attached to the bead, which then binds either to a biotinylated membrane component or to a biotinylated antibody directed against the membrane component, as indicated in Fig. 1. The bead positions at a sequence of equally spaced time points are then recorded by intensified fluorescence video microscopy. The resulting bead trajectories are automatically analyzed by suitable software to obtain the lateral diffusion coefficient, D, of the bead from the dependence of its mean square displacement (MSD or ρ) on the diffusion time.

[1]The following abbreviations are used: SPT: single particle tracking; SBL: supported bilayer; Fl-PE, Bi-PE: Fluorescein-, biotin-conjugated phosphatidylethanolamine; mAb: monoclonal antibody; Fab: antigen-binding fragment of immunoglogulin; GPI: glycosylphosphatidylinositol; FPR: fluorescence photobleaching recovery; LDL: low-density lipoprotein; IgG: immunoglobulin; CCD: charge-coupled device; POPC: 1-palmityoly-2-oleoyl-*sn*-glycero-3-phosphatidylcholine; DOPC: 1,2-dioleoyl-*sn*-glycero-3-phosphatidylcholine; SUV: small unilamellar vesicle; St-bead: streptavidin-conjugated bead; DAF: decay accelerating factor.

An analysis of the stochastic processes which underlie SPT experiments has appeared recently and its predictions are compared to our results (Qian et al., 1991). The fluorescent microbeads used in the present study are about the same size as LDL particles (25 nm) and have about 5% of the mass of the 30 nm gold particles used by Lee *et al.* (1991) and others. One advantage of the polystyrene beads over gold particles is that they are available with different fluorophores dispersed in them, enabling the experimenter to track distinct molecules labeled with beads of different colors in the same experiment. Other advantages are that streptavidin (or other proteins) may be covalently linked to the beads, rather than simply adsorbed as a result of nonspecific hydrophobic interactions and that, under fluorescence epi-illumination, a smaller field depth is achievable than in most bright field microscopy systems.

Materials and Methods

Materials

Probes and Beads

N-((6-(biotinoyl)amino)hexanoyl)-1,2-dihexadecanoyl-*sn*-glycero-3-phosphoethanolamine (Bi-PE) and N-(5-fluoresceinthiocarbamoyl)-1,2-dihexadecanoyl-*sn*-glycero-3-phosphoethanolamine (Fl-PE) were obtained from Molecular Probes (Eugene, OR), as were the sulfate- and carboxyl-modified fluorescent polystyrene latex beads ("FluoSpheres"). The fluorophores in the beads have quantum yields approaching unity and are almost impervious to photobleaching. The beads are available with average diameters from 14 nm to several μm, with a variance of 20% for the smallest and much less for larger beads. Egg lecithin, POPC, DOPC and cholesterol were obtained from Avanti Polar Lipids (Alabaster, AL) and were used without further purification. Streptavidin (St), bovine serum albumin (BSA) and ovalbumin were obtained from Sigma (St Louis, MO).

Streptavidin was covalently coupled to 30 nm carboxyl-modified fluorescent polystyrene latex beads using a water soluble carbodiimide, 1-ethyl-3-(3- dimethylaminopropyl) carbodiimide. The coupling mixture consisted of a 2% suspension of beads (1 ml, approx. 5×10^{15} beads/ml) with 0.5 mg/ml of streptavidin (St : bead molar ratio of 1.0) and a trace amount of ^{125}I-streptavidin, 10 mM carbodiimide, and 20 mM phosphate/carbonate buffer, pH 8.6. After 2 hr at room temperature the reaction was quenched by adding glycine (0.2 M, pH 8.6) and, after 30 min, ovalbumin to 5 mg/ml. The mixture was passed over a 10 ml Sepharose 4B column (Sigma) and was eluted with phosphate buffer (20 mM, pH 7.0, 5 mg/ml ovalbumin) to remove the excess carbodiimide and streptavidin. The beads, which eluted in the void volume of the Sepharose 4B column, contained 10% of the initial ^{125}I-streptavidin radioactivity. Since the coupling efficiency, assayed by the inclusion of tracer I^{125}-St, was about 10%, no more than 1% of the St-coupled beads (St-beads) are expected to carry more than one streptavidin molecule. This should result in minimal aggregation of biotinylated groups by the beads.

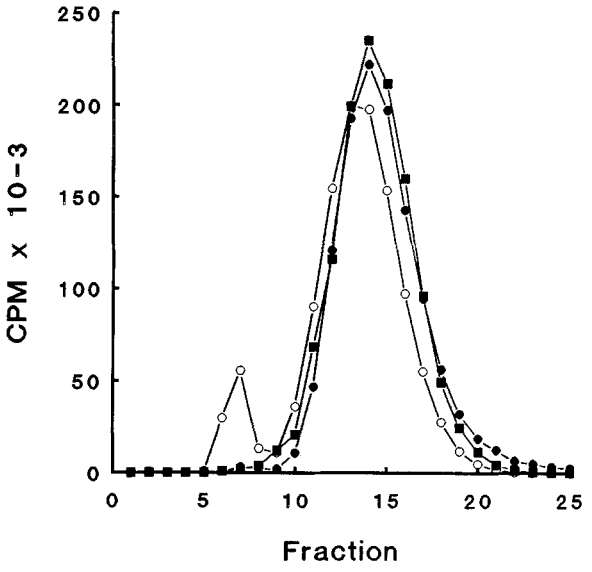

Fig. 2. ○—○: Elution pattern of a suspension of St-beads incubated with biotinylated ^{125}I-3G8 IgG. The beads eluted in the void volume (fractions 6–8), while the larger, later peak arises from the unbound ^{125}I-3G8 IgG. Also shown are: ■—■: the elution pattern of the same quantity of St-beads saturated with an excess of biotin before incubation with the biotinylated ^{125}I-3G8 IgG; and ●—●: the biotinylated ^{125}I-3G8 incubation solution, with no added beads.

The binding capacity of the St-beads for biotinylated proteins was assayed by incubating a suspension of $\approx 8 \times 10^{13}$ beads in PBS buffer with a fivefold molar excess of biotinylated ^{125}I-3G8 IgG (100 μg, 1.3×10^6 cpm). The bead-bound IgG was then separated from the free IgG by passage over a 10 ml Sepharose 4B gel filtration column. The radioactivity associated with each 0.5 ml fraction was then measured and is plotted in Fig. 2. The beads with bound IgG eluted in the void volume of the column (fractions 6–8), while the unbound IgG followed in later fractions. Since approximately 8% of the radioactivity was recovered in the first peak, we conclude that about 40% of the beads had bound an antibody—neglecting the possibility of multiple IgG molecules binding to St, which is tetravalent. It should be noted that the data shown in Fig. 2 were obtained with St-beads prepared under considerably different coupling reaction conditions, including a twofold higher carbodiimide concentration and tenfold higher St and bead concentration than the beads discussed in the preceding paragraph, and that this probably resulted in more efficient St coupling.

Purification of GPI-Anchored Proteins

CD55, the GPI-anchored decay accelerating factor (DAF), was purified from 12 units of blood as described elsewhere (Davitz, Schlesinger & Nussenzweig, 1987). Erythrocytes were lysed by hypotonic shock, hemoglobin was removed from the lysate by ultrafiltration, and the erythrocyte membranes were collected and extracted with butanol. The purification of CD55 in the aqueous phase was accomplished by DEAE ion exchange chromatography, followed by affinity chromatography on an IA10 (anti-CD55 antibody) Sepharose 4B column.

Another GPI-anchored protein, the human Fc receptor FcγRIIIB (CD16), was isolated from RBL-6CD5 cells, a rat basophilic leukemia line transfected with the receptor, obtained from Dr. Jarko Kochan (Hoffmann-La Roche, Nutley, NJ). The cells were grown to confluence, harvested by scraping and, after centrifugation, the cell pellet was washed once in buffer containing 0.5 mM phenylmethyl sulfonyl fluoride (PMSF). Membrane proteins were solubilized with PBS buffer pH 7.4, containing 30 mM β-octyl glucoside, 1 mM PMSF, 5 mM EDTA, 1mM iodoacetamide and 10 μg/ml of the protease inhibitors aprotonin, leupeptin, soybean trypsin inhibitor and pepstatin A. After centrifugation (20 min at 20,000 rpm) to clear debris, the supernatant containing solubilized FcγRIIIB was passed through a 0.45 μm Millipore filter and loaded onto a Sepharose 4B affinity column coupled to the anti-FcγRIIIB monoclonal antibody, 3G8. After extensive washing with PBS containing 0.5 mM PMSF, the retained protein was eluted with 0.1 M glycine HCl, pH 2.3, and the collected fractions were immediately neutralized with 1/10 volume of 1 M Tris-HCl, pH 8.0. Following dialysis, the protein content of the eluted fractions was determined from the absorbance at 280 nm and by use of the BCA reagent. The yield of this purification protocol was 50 μg of protein from 10^9 cells, of which 20% is FcγRIIIB. Assuming that each cell carries 10^6 FcγRIIIB, this is 20% of the theoretical yield.

Purification and Biotinylation of Antibodies

The 4-4-20 hybridoma cells, which produce IgG2a anti-fluorescein antibody (Kranz, Herron & Voss, 1982) were a kind gift of Dr. Voss, University of Illinois. They were grown in Dulbecco's high glucose medium supplemented with 10% fetal calf serum, penicillin (100 U/ml) and streptomycin (100 μg/ml). The antibody was purified from the conditioned medium by passage over a protein-A Sepharose column and the bound 4-4-20 IgG was eluted with 0.1 M glycine-HCl, pH 2.5. The acid eluate was immediately neutralized and dialyzed against PBS. The Fab fragment of 4-4-20 IgG was prepared by digestion (4 hr, 20°C) of the mAb (1 mg/ml) with an equal weight of immobilized papain (Sigma) in 20 mM phosphate buffer, pH 7.0, 10 mM EDTA and 10 mM β-mercaptoethanol, after which the papain was removed by centrifugation. Undigested IgG and Fc fragments were removed by passage over protein-A Sepharose.

The monoclonal antibody against FcγRIIIB, 3G8, and the anti-DAF mAb IA10, a kind gift of Dr. M. Davitz, New York University, were purified according to standard procedures (Fleit, Wright & Unkeless, 1982; Kinoshita et al., 1985).

To biotinylate the 3G8 and IA10 mAb, sulfosuccinimidyl-6-(biotinamido)hexanoate (NHS-LC Bi, Pierce, Rockford, IL) from a 10 mM stock solution in dimethyl sulfoxide was added to IgG (50 μg, 0.1 mM NHS-LC Bi, 20 mM HEPES, pH 8.6, 0.5 ml) and incubated for 1 hr at room temperature. Low molecular weight reaction products were removed from biotinylated IgG by gel filtration over a 10 ml G-25 Sephadex column, eluted with 20 mM HEPES buffer, pH 7.4.

Because direct biotinylation of the mAb in solution inactivated the ligand binding capacity of 4-4-20 IgG or its Fab fragment, the reaction was carried out with the antigen binding site of 4-4-20 mAb protected by binding to a FITC-derivatized lysine-Sepharose 4B column and the bound mAb was reacted *in situ* with 0.1 mM NHS-LC Bi in 20 mM HEPES buffer pH 8.6. After washing the column with several volumes of PBS, bound biotinylated mAb was eluted with 0.1 M glycine-HCl, pH 2.3, neutralized with 0.1 volume of 1.0 M phosphate buffer, pH 8.0, and dialyzed against PBS.

Specimen Chamber and Formation of Glass-Supported Bilayers

Supported bilayers were formed on the coverglass bottom of a specially designed perfusion specimen chamber, using lipid vesicle suspensions with the desired composition. Since the all-glass specimen chamber is thin and flat, it is suitable for high resolution microscopy with either transmitted light or epi-illumination and it may be used with oil-immersion objectives and condensers with high numerical apertures and short working distances. As illustrated in Fig. 3, the chamber has four separate compartments, each with an area of 1.4 mm × 14 mm and a height of 0.2 mm, in which the composition of the perfusion fluid and its flow rate can be controlled by means of syringe pumps.

To obtain reproducible SBL, the coverglasses must be cleaned with care: good results were obtained by immersing them overnight in 20% chromic-sulfuric acid solution ("Chromerge," VWR Scientific, Media, PA), rinsing thoroughly with distilled water, and drying under a nitrogen stream. Small unilamellar vesicles (SUV) of the desired lipid composition were prepared by drying the chloroform/methanol solvent under an argon or nitrogen stream, followed by evaporation of any residual solvent under vacuum for approximately 3 h. PBS buffer was then added and the turbid suspension was placed in a bath sonicator (Model 2200, Branson, Danbury, CT) until it clarified. The vesicle suspension was then drawn into the specimen chamber compartment by a 250 μl syringe pump and after allowing a bilayer to form (about 15 min), the excess vesicles were removed by rinsing with PBS containing 5 mg/ml of BSA. Finally, the SBL was incubated with the appropriate mAb (15 min) and after rinsing with the same buffer to remove excess mAb, the St-beads were added in the presence of BSA and rinsed again.

Image Acquisition and Analysis

Fluorescence images of sulfate-modified "red" beads with nominal diameters (2R) of 22, 30, 50 and 121 nm, immobilized on a polylysine coated coverglass were obtained by use of an Axiovert inverted microscope (Carl Zeiss, Thornwood, NY), a 100×, 1.3 N.A. Neofluar objective and a cooled slow-scan CCD camera (Astromed, Cambridge, UK); excitation and emission interference filters centered at 560 (band width 40 nm) and 630 nm (band width 23 nm), respectively, and a dichroic mirror centered at 595 nm (Omega Optical, Brattleboro, VT) were used. Figure 4 shows the intensity profiles of individual 22 and 121 nm beads together with the best fit to a Gaussian function. The full width at half maximum of the images of all beads with average diameters up to 121 nm were found to be about 3 pixels, corresponding to ≈450 nm. This value is comparable to the diffraction limited resolution $w = 1.22\ \lambda_0/\mathrm{NA} \sim 550$ nm, where λ_0 is the vacuum wavelength of the emitted light and NA is the numerical aperture of the objective used in the measurement (Keller, 1989). The peak fluorescence intensities of 15–20 individual beads were averaged to obtain the intensities I_{av}, which are shown plotted against average bead volume in Fig. 5. Since the widths of the fitted Gaussians were independent of the bead diameter (*cf.* Fig. 4), the peak and total fluorescence intensities are proportional to each other, so that the linear relationship of Fig. 5 is an indication

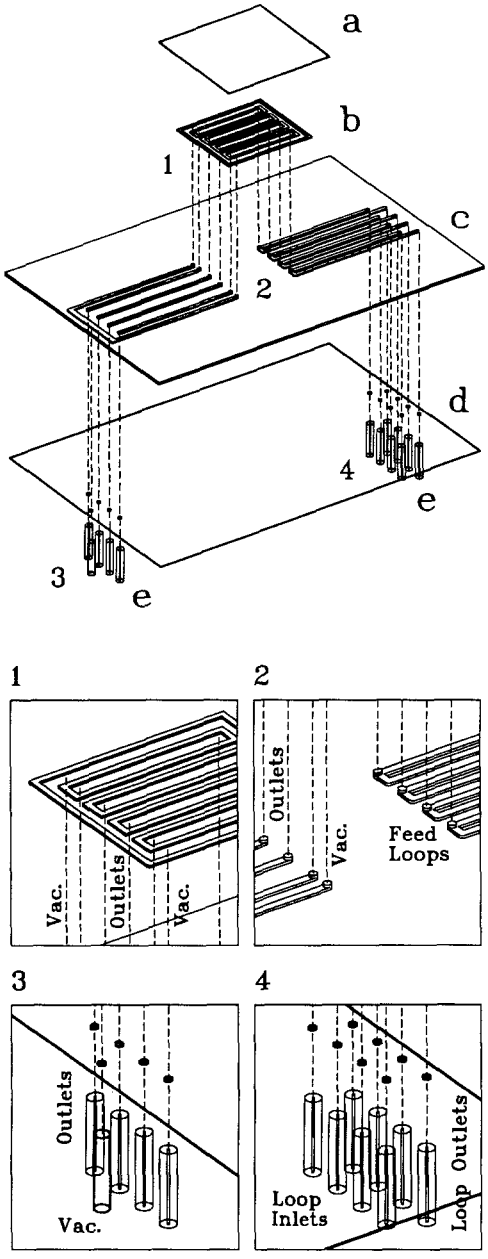

Fig. 3. Exploded view of the four-compartment perfusion chamber. The coverglass *a* (0.17 mm thick, 22 mm sq) is held in place by vacuum applied to the space between the outermost square gasket and the four rectangularly shaped gaskets (*b*) which define the compartments (detail *1*). The gaskets are 0.2 mm in height and are bonded to the glass plate *c* (0.7 mm thick); the opposite side of plate *c* is engraved with grooves which form conduits for the perfusant when *c* is bonded to plate *d* (0.2 mm thick). The perfusant enters one end of a particular compartment from a feed loop conduit by way of a hole drilled through *c*, and is drawn into the outlet conduit through a hole at its other end (detail *2*). Perfusant reservoirs are connected to the chamber by flexible tubing attached to connectors which are bonded to plate *d* (details *3* and *4*). Vacuum for attaching the coverglass is provided to the chamber in a similar manner. When used with an inverted microscope, as in this work, the chamber is inverted from the position shown here. The chamber is itself held in place on the temperature-controlled microscope stage by vacuum (*not shown*).

that the fluorophores are uniformly distributed within the volume of the bead and not confined to its surface.

In the SPT experiments, the positions of individual beads were recorded at successive time intervals by use of an intensified video CCD camera (Model C2400, Hamamatsu, Bridgewater, NJ). In this work, single-frame (33 msec) bead images were acquired at a rate of 5 sec^{-1} with the aid of an 8-bit image analysis program (Image 1, Universal Imaging, Media, PA) and stored on an optical disc recorder (Panasonic TQ3038F), but higher acquisition rates, up to 30 frames/sec, may be used if necessary. After background subtraction, image contrast enhancement and thresholding, the bead coordinates were determined by a centroid algorithm to a nominal precision of 0.1 μm, the true precision depending on the signal/noise ratio of the bead image.

The trajectories were automatically derived from the bead coordinates by use of a program written by Dr. A. Ishihara and kindly provided to us by Dr. K.A. Jacobson, University of North Carolina. To trace the path of an individual bead, the program searches within each frame for beads whose coordinates are within a user-defined distance of a bead position recorded in the preceding frame.

Since stochastic processes are responsible for the Brownian motion of a particle, its diffusion coefficient (D) can be derived from the time dependence of its mean square displacement (Einstein, 1905) and its precision is limited by the statistical variance, even if all time and position measurements used to define its trajectory were free of experimental errors. The accuracy of D therefore increases with the number of time and position observations.

Qian *et al.* (1991) calculated the dependence of the statistical variance of the MSD on the number of observations defining the trajectory of a particle. According to their derivation, if $\mathbf{r}(t)$ is the position of the particle at time $t = n\Delta t$, where Δt is the time interval between consecutive position determinations, its displacement from its initial position is $\mathbf{r}(t) - \mathbf{r}(0)$. It can then be shown from fundamental considerations (Berg, 1983) that $\rho(t)$, the mean square displacement of a particle for a diffusion interval t, is

$$\rho(t) \equiv \langle |\mathbf{r}(t) - \mathbf{r}(0)|^2 \rangle = 4Dt \tag{1}$$

where the average is taken over all independent measurements of the displacement.

If the number of positions defining the bead trajectory (not counting the initial position at time $t = 0$) is N, then the number of independent determinations of $\rho(\Delta t)$ is N, the number of determinations of $\rho(2\Delta t)$ is $N - 1$, and generally, the number of independent measurements for a time interval $t = n\Delta t$, is $\rho(t) = N - n + 1$; for the longest diffusion time, $t = N\Delta t$, only a single measurement of ρ is available. $\Delta\rho(t)$, the time dependence of the standard deviation of $\rho(t)$, can then be shown to be (Qian et al., 1991):

$$\Delta\rho(t) = 4Dn\Delta t \sqrt{\frac{2n^2 + 1}{3n(N - n + 1)}} \tag{2}$$

This equation gives the statistical error associated with each time point, $n\Delta t$. Usually only those time intervals for which a large number of observations are available are included in the analysis; in that case, $N \gg n$, and using Eq. (1), Eq. (2) may be simplified to

$$\frac{\Delta\rho(t)}{\rho(t)} \approx 0.8\sqrt{\frac{n}{N}} \tag{3}$$

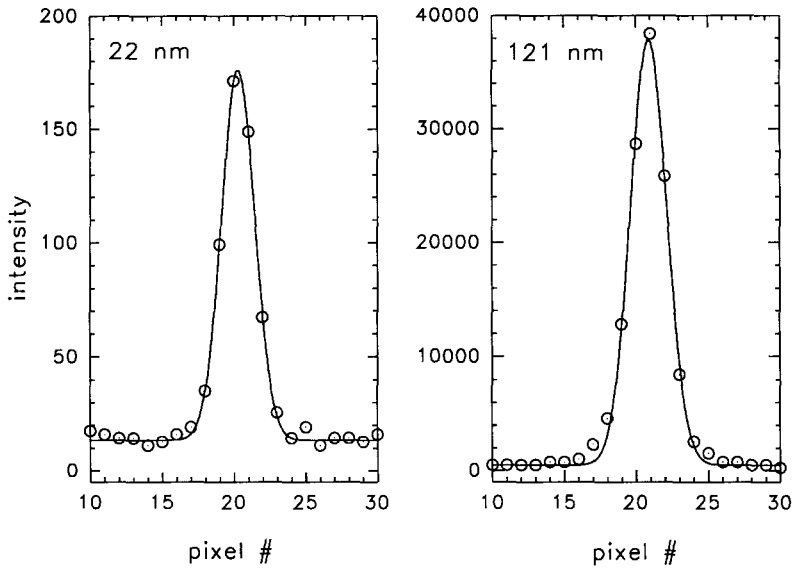

Fig. 4. Fluorescence intensity profiles of bead images (diameter 22 and 121 nm) acquired with a slow-scan cooled CCD camera. With each CCD pixel imaging an area of 0.15 × 0.15 μm, the full width at half maximum is seen to be 0.45 μm for both images.

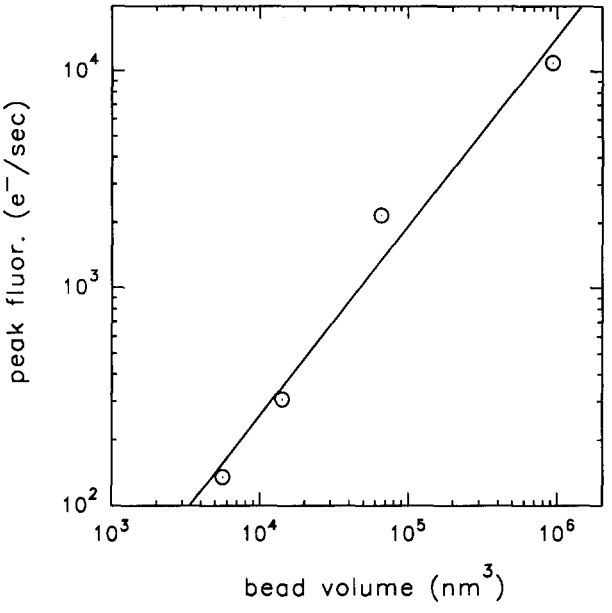

Fig. 5. Dependence of the maximum bead fluorescence intensity (in CCD electrons/s) on bead volume (in nm^3). Fluorescence images of immobilized red FluoSpheres, with nominal average diameters from 22 to 121 nm, were acquired by a slow-scan cooled CCD camera using a Zeiss 100×, 1.3 NA Neofluar objective (*cf.* Fig. 5). The fluorescence intensities shown represent average values for 20 beads.

D is determined according to Eq. (1) from the slope of the best fit straight line of $\rho(t)$ *vs.* t, with each point weighted inversely to $\Delta\rho$. Thus, if 500 successive observations are used to define the track of a particular bead, the error in the calculated $\rho(t)$ for all available intervals up to 30 Δt in duration is expected to be below 20%, according to Eq. (3). This uncertainty is reduced if the MSD data for many trajectories are combined, with the assumption that all beads and their linkages are identical and that the bilayer is homogeneous.

However, if the diffusion of the particle is limited to a range of magnitude R, e.g., by membrane heterogeneities or boundaries, $\rho(t)$ will be a linear function of t only for $t < t_{max}$. The diffusion range of the particle may then be estimated to be of the order of $R \approx 2\sqrt{(Dt_{max})}$, where D is the diffusion coefficient derived from the initial, linear portion of $\rho(t)$ (*cf.* Eq. 1). In the case of proteins diffusing in a membrane, a $\rho(t)$ plot which levels off for long diffusion times (i.e., $d^2\rho/dt^2 < 0$) may be due to diffusion barriers or to "molecular crowding" or to the presence of repulsive or attractive interactions between the diffusing molecules (Scalettar & Abney, 1991). A $\rho(t)$ plot with positive curvature, on the other hand, is indicative of flow or drift in the membrane.

Results

Accessibility of Fluorescein Hapten

The mAb 4-4-20 binds fluorescein with an equilibrium association constant $K_a = 1.7 \times 10^{10}$ M^{-1} and binding results in 96% quenching of the hapten fluorescence (Kranz et al., 1982). Therefore, the measurement of the reduction of the fluorescein fluorescence intensity in the presence of the mAb provides a simple and sensitive assay of antibody integrity. Figure 6 compares the results of titrations of native and biotinylated mAb 4-4-20 with fluorescein in solution: the similarity of the two curves demonstrates that our method for biotinylating the mAb while protecting its active site preserves the full binding capacity of the antibody.

However, it was recently reported that the fluorescein moiety of Fl-PE is only *partially* accessible when incorporated in POPC monolayers and bilayers (Ahlers et al., 1992). Furthermore, experiments by Petrossian and Owicki (1984) showed that

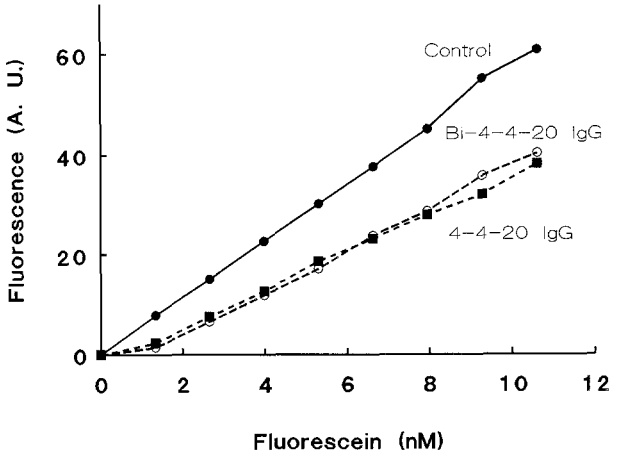

Fig. 6. Fluorescence titration of fluorescein in HEPES, 0.02 M, pH 7.5, in the absence and presence of either native or biotinylated mAb 4-4-20, both at a concentration of 3.3 nM. Note that when 4-4-20 IgG was reacted with 0.1 mM NHS-LC Bi *without* binding site protection (*cf.* Materials and Methods), no fluorescence quenching took place.

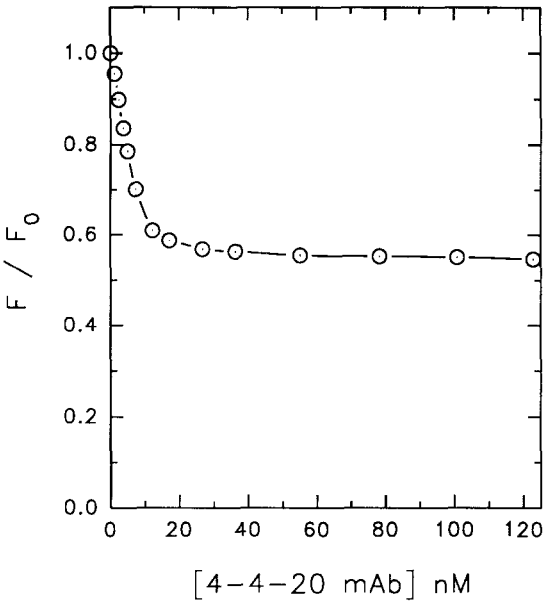

Fig. 7. Fluorescence quenching of Fl-PE dispersed at a probe : lipid ratio of 0.002 in 50 μM DOPC SUV. F_0 and F represent the fluorescence intensity in the absence and in the presence of increasing amounts of mAb, respectively.

the accessibility of fluorescein may also depend on the chemical nature of the matrix lipids. We therefore investigated whether the fluorescein moiety of Fl-PE constitutes an effective hapten for bead attachment in supported bilayers. DOPC SUV, 50 μM lipid containing 0.2 mol % of Fl-PE, were formed by extensive bath sonication under argon, and the fraction of fluorescein accessible to quenching was determined by titrating the vesicle suspension with mAb 4-4-20. Fluorescence spectra were measured with a laboratory-modified SLM spectrofluorometer (SLM, Urbana, IL). The accessible fraction was, as expected, less than unity, since in SUV about half of the probes are in the inner leaflet and, moreover, some vesicles may be multilamellar. In our experiments approximately 40–45% of the total fluorescence was quenched by the antibody (*cf.* Fig. 7), which suggests that about 80–90% of the outer leaflet haptens are accessible to 4-4-20. A similar experiment was carried out on a DOPC/Fl-PE supported bilayer. The fluorescence of Fl-PE was measured at sufficiently low excitation light intensity to prevent photobleaching using a slow-scan cooled Model 1530P EG&G CCD camera (EG&G-PARC, Princeton, NJ). Exchange of the buffer with a 100 nM solution of biotinylated mAb 4-4-20, a saturating concentration, resulted in approximately 33% quenching of the initial fluorescence at equilibrium, indicating that 65–70% of the haptens in the upper leaflet of the SBL are available for binding by the biotinylated mAb.

Mobility of Lipid Analogues

One of the objectives of the present investigation is to evaluate the SPT methodology for measuring lateral diffusion coefficients, D, and compare these values with those obtained by other established methodologies. Glass-supported bilayers constitute convenient model systems for these studies because they can be formed readily with any lipid, they undergo temperature-induced phase transitions, and GPI-linked and other proteins may be inserted in them (Zhang et al., 1992). While antibody-linked beads have wide applicability, the simplest specific bead-lipid linkage is obtained by use of a biotinylated lipid analogue and a streptavidin-coupled bead.

SBL were formed as described above, using SUV of egg lecithin : cholesterol (molar ratio 80 : 20) containing Bi-PE at a molar probe : lipid ratio (x) between 10^{-4} and 10^{-2}. After rinsing the bilayer, St-beads were admitted to the chamber compartment and allowed to bind to Bi-PE before further rinsing. Beads attached to the planar SBL remained in focus for several minutes; unattached beads diffused in and out of focus at a much faster rate. Mock-derivatized beads (St omitted from the coupling reaction mixture) did not bind, St-beads did not bind if Bi-PE was not present in the SBL and addition of biotin to the St-beads blocked subsequent binding to Bi-PE in the bilayer. Invariably, some beads attached to the bilayer without diffusing. The mobile fraction varied from 10 to 50% in different SBL and the cause for this variability is under continuing investigation.

Figure 8 shows a typical trajectory of a Bi-PE-

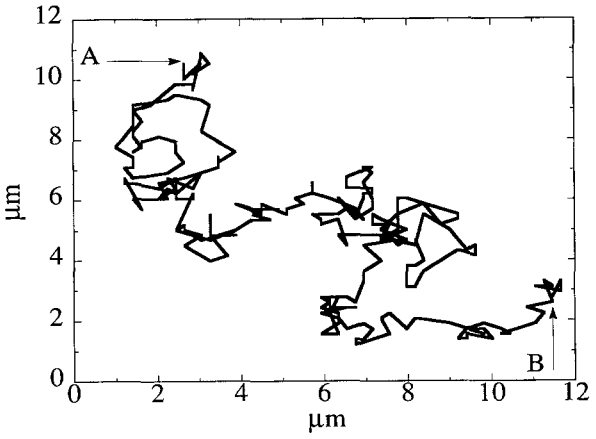

Fig. 8. Typical trajectory of a 30 nm fluorescent bead linked to Fl-PE in an egg lecithin : cholesterol (80 : 20) supported bilayer. The bead positions were determined 5 times a second.

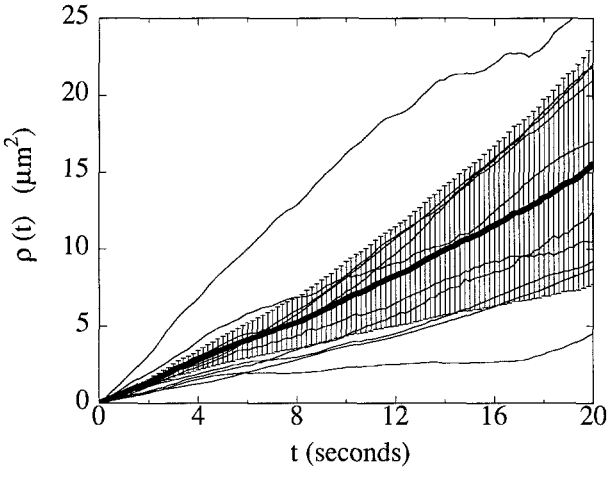

Fig. 9. Dependence of the mean square displacement on diffusion time, $\rho(t)$, for 10 individual 30 nm beads tethered to Fl-PE in an egg lecithin : cholesterol (80 : 20) bilayer is shown by the 10 light curves. Bead positions were recorded at a rate of 5 sec^{-1} for a total observation time of 50 sec. Also shown is the MSD averaged over all 10 beads (heavy curve) and its theoretical standard deviation, $\Delta\rho(t)$, calculated according to Eq. (3) with $N = 250$.

linked St-bead and Fig. 9 shows individual $\rho(t)$ plots for 10 beads and their average. From the slope of the straight line fitted to such data for diffusion times from 0.2 to 10 sec, D was determined according to Eq. (1). Figure 9 also shows that the expected standard deviation, $\Delta\rho(t)$ (*cf.* Eq. 3), is consistent with the observed variability in $\rho(t)$ among the individual beads.

Figure 10 shows histograms of the values of D obtained for this system using SBL with three Bi-PE mole fractions, as well as their average values, $\langle D\rangle$. The dependence of D on x is seen to be small.

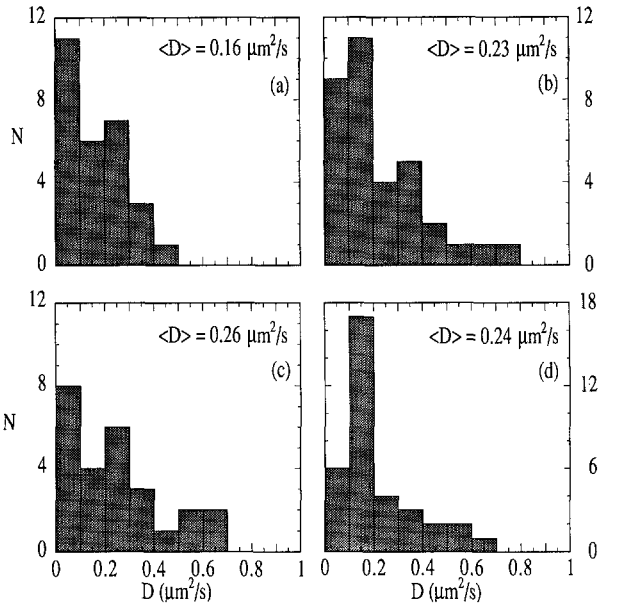

Fig. 10. (*a–c*) Distribution of D values and their average $\langle D\rangle$ for St-beads linked to Bi-PE in egg lecithin : cholesterol (80 : 20) bilayers at molar probe ratios, $x = 10^{-2}$, 10^{-3} and 10^{-4}, respectively. N is the number of beads. (*d*) Distribution of D values and their average, $\langle D\rangle$, for bead-linked Fl-PE at a molar probe ratio of $x = 10^{-3}$ in a SBL of the same composition as above. The diffusivity of the phospholipid linked to St-beads by biotinylated mAb 4-4-20 does not differ significantly from the beads in *b*, whose linkage to the SBL is shorter (*cf.* Fig. 1).

The same figure also shows values of D for Fl-PE dispersed in a SBL of the same composition at $x = 10^{-3}$ and linked to St-beads by use of the biotinylated mAb 4-4-20. Similar results were obtained when the Fab fragment was used instead of the mAb. The value of $\langle D\rangle$ does not differ significantly from that for Bi-PE, in spite of the somewhat bulkier bead linkage required for Fl-PE. We also compared the diffusivities of bead-linked Fl-PE in lecithin SBL containing 0 and 20 mol% cholesterol and observed no difference within the experimental uncertainties. This finding is consistent with similar results obtained by FPR (Rubenstein, Smith & McConnell, 1979).

These values for $\langle D\rangle$ are comparable to those for Fl-PE in analogous SBL, obtained by Lee *et al.* (1991) by tracking 30 nm gold particles coated with anti-fluorescein antibodies by bright field video microscopy. The diffusion coefficient of Fl-PE in similar SBL measured by FPR, however, was reported to be several times higher ($D = 1.3$ μm^2/sec) (Lee et al., 1991) and possible reasons for this difference are discussed below.

Mobility of GPI-Anchored Proteins

Incubation of purified DAF (CD55) and FcγRIIIB (CD16) in PBS in the *absence* of β-octyl glucoside

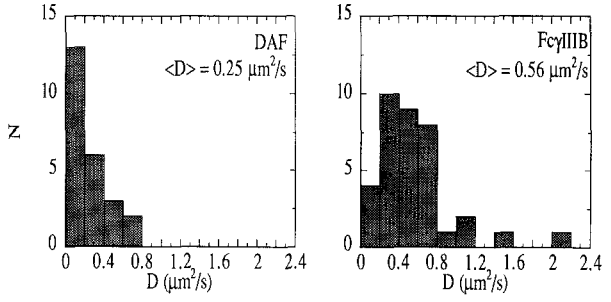

Fig. 11. Histograms showing the values of D and their average, $\langle D \rangle$, for bead-linked GPI-anchored proteins CD55 and FcRγIIIB, both dispersed in egg lecithin : cholesterol (80 : 20) supported bilayers.

with preformed SBL (egg lecithin : cholesterol, 80 : 20 molar ratio) resulted in the spontaneous insertion of the proteins into the bilayer. The movement of these GPI-anchored proteins in the bilayer was tracked by attaching them to St-beads by means of their respective biotinylated mAb, as was done with Fl-PE. The trajectories were acquired and analyzed as described above and the distributions of D and $\langle D \rangle$ values shown in Fig. 11 were obtained. $\langle D \rangle$ values for the bead-tethered CD55 and FcγRIIIB receptors in the SBL were 0.25 and 0.56 μm^2/sec, respectively. For comparison, the FPR value of D for CD55 labeled with the fluorescein-conjugated anti-CD55 mAb IA10 in HeLa cell membranes was reported to be 0.16 μm^2/sec (Thomas et al., 1987), while the values for several other GPI-anchored proteins measured by FPR have been reported to be of the same order of magnitude, ranging from 0.1 to 0.5 μm^2/sec (Low, 1989; Zhang et al., 1992).

Discussion

In this report we have presented a general methodology for determining the mobility of membrane constituents by tethering them to fluorescent microbeads. While the present work deals only with SBL model membranes, preliminary experiments indicate that the technique is also applicable to intact cell membranes, where it may shed light on the distribution, transport and diffusive properties of specific membrane molecules, although the effect of the cell's glycocalyx on the mobility of tethered beads remains to be evaluated.

In the SBL model systems the St-beads were found to bind with high specificity and rarely became detached, but the mobile fraction was variable, possibly because of beads immobilized on glass at bilayer imperfections. Since the mobility of an individual bead is likely to be seriously hindered by simultaneous binding to several membrane constituents, the "multi-valency effect" (Lee et al. 1991), we prepared the St-beads so that the average number of streptavidin molecules per bead was less than unity. However, despite our precautions, the possibility that some of the observed beads were attached to the bilayer by more than one linkage cannot be excluded.

The average diffusion coefficients of beads linked to the lipid analogues Bi-PE and Fl-PE were found to be 0.26 and 0.24 μm^2/sec, respectively, or about one-fifth of that for Fl-PE in a similar SBL, as measured by FPR for similar diffusion distances. The reasons why the lipid analogue diffuses more slowly when tethered to a bead are not clear: They include the drag imposed by the bead and its linker in the aqueous phase, although it has been reported that doubling the viscosity of the aqueous compartment has no effect on the diffusivity of gold particles attached to a bilayer (Lee et al., 1991). It is also possible that electrostatic interactions between the latex beads and the bilayer retard the diffusive motion of tethered beads, although we could not observe any ionic strength dependence effect for concentrations of NaCl between 10 and 150 mM. Our $\langle D \rangle$ values are comparable to those obtained by Lee *et al.* (1991) for Fl-PE in similar bilayers by SPT of tethered gold particles. In addition to "multi-valency," other possible reasons for the lower mobility values measured by SPT are being explored.

The effective diffusivities of the two bead-linked GPI-anchored proteins, on the other hand, is of the same order of magnitude as those obtained by FPR experiments. While this may be related to the fact that the linkage to the bead-linked protein moieties consists of 5 sugar moieties (Low, 1989) and appreciably longer than it is in the case of the two lipid analogues (*cf.* Fig. 1), we saw no significant dependence of $\langle D \rangle$ on the nature of the linkage for lipid analogues, as illustrated in Fig. 10. The lateral mobility of these proteins is of considerable interest since the mode of attachment of the GPI anchor to the C-terminal amino acid and the structure of the anchor are remarkably similar in proteins which differ substantially in function and origin. The ubiquity of GPI-anchored proteins suggests that they are endowed with physiologically important functions based on their mobility and their enhanced capacity for interacting with other membrane proteins (Low, 1989). The methodology presented here provides a tool for investigating the mechanism of action of these proteins.

This work was supported by National Institutes of Health grants 1R24 RR05272 and AI-24322.

References

Ahlers, M., Grainger, D.W., Herron, J.N., Lim, K., Ringsdorf, H., Salesse, C. 1992. Quenching of fluorescein-conjugated lipids by antibodies. *Biophys. J.* **63**:823–838

Anderson, C.M., Georgiou, G.N., Morrison, I.E.G., Stevenson, G.V.W., Cherry, R.J. 1992. Tracking of cell surface receptors by fluorescence digital imaging microscopy using a charge-coupled device camera. Low density lipoprotein and influenza virus receptor mobility at 4 C. *J. Cell Sci.* **101**:415–425

Axelrod, D. 1983. Lateral motion of membrane proteins and biological function. *J. Membrane Biol.* **75**:1–10

Axelrod, D., Koppel, D., Schlessinger, J., Elson, E., Webb, W.W. 1976. Mobility measurements by analysis of fluorescence recovery after photobleaching. *Biophys. J.* **16**:1055–1069

Berg, H.C. 1983. Random Walks in Biology. Princeton University Press, Princeton, NJ

Bretscher, M.S. 1984. Endocytosis: relation to capping and cell locomotion. *Science* **224**:681–686

Curtain, C.C., Gordon, L.M., Aloia, R.C. 1988. Lipid domains in biological membranes: Conceptual development and significance. *In:* Lipid Domains and the Relationship to Membrane Function. R.C. Aloia, C.C. Curtain, and L.M. Gordon, editors. pp. 1–15. Alan R. Liss, New York

Davitz, M.A., Schlesinger D., Nussenzweig, V. 1987. Isolation of decay accelerating factor (DAF) by a two-step procedure and determination of its N-terminal sequence. *J. Imm. Methods* **97**:71–76

De Beus, A., Eisinger, J. 1992. Modulation of lateral transport of membrane components by spatial variations in diffusivity and solubility. *Biophys. J.* **63**:607–615

DeBrabander, M., Nuydens, R., Ishihara, A., Holifield, B., Jacobson, K., Geerts, H. 1991. Lateral diffusion and retrograde movements of individual cell surface components on single motile cells observed with nanovid microscopy. *J. Cell Biol.* **112**:111–124

Edidin, M., Kuo, S.C., Sheetz, M.P. 1991. Lateral movements of membrane glycoproteins restricted by dynamic cytoplasmic barriers. *Science* **254**:1379–1382

Edidin, M., Stroynowski, I. 1991. Differences between the lateral organization of conventional and inositol phospholipid-anchored membrane proteins. A further definition of micrometer scale membrane domains. *J. Cell Biol.* **112**:1143–1150

Edwards, C., Frisch, H.L. 1976. A model for the localization of acetylcholine receptors at the muscle endplate. *J. Neurobiol.* **7**:377–381

Einstein, A. 1905. Ueber die von der molecularkinetischen Theorie der Wärme geforderte Bewegung von in ruhenden Flüssigkeiten suspendierten Teilchen. *Ann. d. Physik* **17**:549–560

Eisinger, J., Flores, J., Petersen, W.P. 1986. A milling crowd model for local and long-range obstructed lateral diffusion—Mobility of excimeric probes in the membrane of intact erythrocytes. *Biophys. J.* **49**:987–1001

Eisinger, J., Halperin, B.I. 1986. Effects of spatial variation in membrane diffusibility and solubility on the lateral transport of membrane components. *Biophys. J.* **50**:513–521

Fahey, P.F., Webb, W.W. 1978. Lateral diffusion in phospholipid bilayer membranes and multilamellar liquid crystals. *Biochemistry* **17**:3046–3053

Fleit, H.B., Wright, S.D., Unkeless, J.C. 1982. Human neutrophil Fc gamma receptor distribution and structure. *Proc. Natl. Acad. Sci. USA* **79**:3275–3279

Geerts, H., De Brabander, M., Nuydens, R., Geuens, S., Moeremans, M., De Mey, J. Hollenbeck, P. 1987. Nanovid tracking: A new automatic method for the study of mobility in living cells based on colloidal gold and video microscopy. *Biophys. J.* **52**:775–782

Ghosh, R.N., Webb, W.W. 1990. Evidence for intra-membrane constraints to cell surface LDL receptor motion. *Biophys. J.* **57**:286*a*

Gross, D.J., Webb, W.W. 1988. Cell surface clustering and mobility of the liganded LDL receptor measured by digital video fluorescence microscopy. *In:* Spectroscopic Membrane Probes. L.M. Loew, editor pp. 19–45 CRC, Boca Raton, FL

Haverstick, D.M., Glaser, M. 1988. Visualization of domain formation in the inner and outer leaflets of a phospholipid bilayer. *J. Cell Biol.* **106**:1885–1896

Keller, H.E. 1989. Objective lenses for confocal microscopy. *In:* The Handbook of Biological Confocal Microscopy. J. Pawley, editor. pp. 69–77. IMR, Madison, WI

Kinoshita, T., Medof, M.E., Silber, R., Nussenzweig, V. 1985. Distribution of decay-accelerating factor in the peripheral blood of normal individuals and patients with paroxysmal nocturnal hemoglobinuria. *J. Exp. Med.* **162**:75–92

Kranz, D.M., Herron, J.N, Voss, E.W., Jr. 1982. Mechanisms of ligand binding by monoclonal anti-fluorescyl antibodies. *J. Biol. Chem.* **257**:6987–6995

Lee, G.M., Ishihara, A., Jacobson, K.A. 1991. Direct observation of Brownian motion of lipids in a membrane. *Proc. Natl. Acad. Sci. USA* **88**:6274–6278

Low, M.G. 1989. The glycosyl-phosphatidylinositol anchor of membrane proteins. *Biochim. Biophys. Acta* **988**:427–454

Petrossian, A., Owicki, J.C. 1984. Interaction of antibodies with liposomes bearing fluorescent haptens. *Biochim. Biophys. Acta* **776**:217–227

Qian, H., Sheetz, M.P., Elson, E.L. 1991. Single particle tracking—Analysis of diffusion and flow in two-dimensional systems. *Biophys. J.* **60**:910–921

Rodgers, W., Glaser, M. 1991. Characterization of lipid domains in erythrocyte membranes. *Proc. Nat. Acad. Sci. USA* **88**:1364–1368

Rubenstein, J.L.R., Smith, B.A., McConnell, H.M. 1979. Lateral diffusion in binary mixtures of cholesterol and phosphatidylcholines. *Proc. Natl. Acad. Sci. USA* **76**:15–18

Sassaroli, M., Vauhkonen, M., Perry, D., Eisinger, J. 1990. The lateral diffusivity of lipid analogue excimeric probes in dimyristoylphosphatidylcholine bilayers. *Biophys. J.* **57**:281–290

Scalettar, B.A., Abney, J.R. 1991. Molecular crowding and protein diffusion in biological membranes. *Comments Mol. Cell. Biophys.* **7**:79–107

Singer, S.J., Nicolson, G.L. 1972. The fluid mosaic model of the structure of cell membranes. *Science* **175**:720–731

Taylor, R.B., Duffus, P.H., Raff, M.C., de Petris, S. 1971. Redistribution and pinocytosis of lymphocyte surface immunoglobulin molecules induced by anti-immunoglobulin antibody. *Nature New Biol.* **233**:225–229

Thomas, J., Webb, W., Davitz, M.A., Nussenzweig, V. 1987. Decay accelerating factor diffuses rapidly on HeLa(AE) cell surfaces. *Biophys. J.* **51**:522*a*

Yechiel, E., Edidin, M. 1987. Micrometer-scale domains in fibroblast plasma membranes. *J. Cell Biol.* **105**:755–760

Zhang, F., Schmidt, W.G., Hou, Y., Williams, A.F., Jacobson, K. 1992. Spontaneous incorporation of the glycosyl-phosphatidylinositol-linked protein Thy-1 into cell membranes. *Proc. Natl. Acad. Sci. USA* **89**:5231–5235